Prediction of Mine Face Ventilation using Computational Fluid Dynamics

University of Kentucky

June 27, 2002

Introduction

This report includes results from analyses performed using CFD (Computational Fluid Dynamics) for the purpose of predicting the flow within an open face mine. Several scenarios are explored to compare the CFD results to experimental data taken with PIV (Particle Image Velocimetry). Up to this point, only one commercial CFD program, Fluent, has been utilized but other commercial and non-commercial codes should be tested. If a CFD program is found to effectively predict the flow in the mine face, then the program can be used to make advancements in mine ventilation technology. New products could be developed faster and cheaper by minimizing the amount of required experimentation.

There were four major scenarios examined with PIV by Wala and Jacob at the University of Kentucky. These scenarios were then analyzed using the commercial CFD software package, Fluent. The objective was to fully utilize the software's many features to obtain an accurate prediction of the onset separation that occurs during three of the four scenarios. This separation of the flow prevents proper ventilation near the face and allows for methane build-up at cutting face. The build-up of methane at the cutting face increases the probability that an explosion will occur and should be prevented by proper ventilation. If CFD can predict the onset separation that occurs, new ways of preventing the separation can be developed on the computer instead of making expensive prototypes and using expensive test equipment.

1 Background

1.1 Four Mining Scenarios

Four scenarios were examined to simulated the process of coal extraction from a mine face. In all scenarios the geometry of the mining vehicle was excluded for the purpose of simplifying the modeling procedure. The path by which the remote control miners take during normal operation was broken into four main geometries including (a) 30 foot box cut, (b) 30 foot slab cut, (c) 60 foot box cut and (d) 60 foot slab cut. Illustrated in figure1 are the geometries along with the dimensions for the full scale mine face.

1.2 Experimental Data (PIV)

Experiments were performed using PIV to generate two-dimensional plots of velocity-vectors, velocity contours, vorticity contours, etc. These two-dimensional plots were taken in the horizontal plane that is offset from the bottom at a distance equivalent to half of the total height. This plane will be referred to as the mid-plane throughout this report. For more details on the experimental data see the report by Wala[1]. Figure 2 are the velocity-vector plots yielded by PIV for the previously mentioned scenarios.

2 Setup

2.1 Grid Generation

Grid generation for CFD simulations is a very important component of the analysis setup. Two main points were considered while generating grids for each case including the shape of cells and the size of cell near the walls. First, a non-uniform structured grid, composed only of quadrilateral cells, was used for all simulations presented in this report. Second, the size of the grid cell near the wall is calculated based on the value of y^+ recommended for the turbulence model being used. For details on this calculation, see the Fluent User's Guide[2].

2.2 Grid Sensitivity Study

Because the solution of an analysis can be dependent on how the model is discretized, it is proper procedure to seek a grid-independent solution before accepting any results with confidence. A grid-independent solution is achieved by performing a grid-sensitivity study which ensures that mesh, or grid, will no longer affect the solution. A grid-sensitivity study is performed by comparing the results of three differently sized grids. The original grid should be modified by increasing the total number of points while conserving the ratios of the points in each direction. For example, brick A contains 1000 grid cells, or points, with 10 points in the x-direction, 5 in the y-direction and 20 in the z-direction. To create brick B by doubling the total number of cells while conserving the ratios of the cells in each direction, the number of cells in each direction must be multiplied by $\sqrt[3]{2}$ or $1.25992105 \approx 1.26$. If the results from the three grids compare well, then the solution is considered to be grid-independent.

> *Note that a grid-independent solution has been reached for some of the following results but not for all.*

2.3 Boundary Conditions

Because we were attempting to match our results with PIV results, the boundary conditions of the model were very important. All scaling is done by keep the Reynold's number constant and adjusting the velocity to compensate for the smaller geometry. An inlet velocity of 28 m/s is used to simulate the velocity generated by the seeded fan system on the PIV setup[1]. Next, the density and viscosity are those found for air at room temperature in BASIC FLUID MECHANICS[3], which are 1.20 kg/m^3 and $1.51 \cdot 10^{-5}$ m^2/s, respectively. Also, the roughness on the walls was assumed to be $1 \cdot 10^{-5}$ to represent the plexiglas that was used in the PIV model. Finally, other parameters are specific to the turbulence model used.

There are many different methods to model the turbulence and some ways are more effective than others depending on the application. Also, some turbulence models are more easily converged than others. The Reynolds Average Numerical Simulation (RANS) models are usually faster but are only accurate in certain applications and geometries. Three RANS turbulence models including the Standard $k-\varepsilon$, Spalart-Allmaras and Shear-Stress Transport $k-\omega$ models were used and the results were compared to find the most robust and most accurate model.

Because the $k-\varepsilon$ model allows the use of a standard wall function, it is possible to decrease the total number of grid points by assuming the boundary layer can be predicted with one equation. Fluent recommends a $y^+ \geq 30$ while using the standard wall function, thus the calculated grid size for the cells near the wall is a dimensionless value of $.01722 \approx .035ft$. Next, the boundary condition parameter k and ε are used to represent turbulence kinetic energy and turbulence dissipation rate, respectively. Another important parameter is the

turbulent viscosity, μ_t, which we assume to be 10% of the reference viscosity. The relationship between these three parameters is given in the Fluent User's Guide[2] as $\mu_t = \rho C_\mu \frac{k^2}{\varepsilon}$, where $C_\mu = .09$ is constant. k is given the value of 1.96 m^2/s^2 and ε is calculated to be 229,000 m^2/s^3.

The Spalart-Allmaras and $k-\omega$ SST models have similar grids, however, the boundary condition parameters for turbulence are different. There is only one parameter for the S-A model, which is $\mu_t = 0.1 * \mu_{ref}$. The SST model contains two parameters for modeling turbulence k and ω. k is the same term that was given for the $k-\varepsilon$ model and ω is related with the equation:

$$\omega = \varepsilon/(C_\mu k)$$

3 Results

3.1 Convergence

Because the analysis that was performed in this report implicitly solved a set of segregated partial differential equations, an iterative solution was yielded. When solving equations iteratively, there is usually some imbalance of continuity and momentum equations by which we quantify in this case with the residuals. As the CFD program completes more iterations, the residual plot for the solution should yield a negatively sloped curve. As the curve continues to drop, the slope should approach zero creating a horizontal line. Once the residual plot has flattened for more than 1000 iterations the value of the residual should be checked. If the value of the residual at the flat line is less than 10^{-3}, a value recommended by Fluent, then the solution can be considered converged.

3.2 The $k-\varepsilon$ Model

3.2.1 30 FOOT BOX CUT

A grid-independent solution was found for the 30 foot box cut scenario using the $k-\varepsilon$ model with a standard wall function. Three grid sizes were solved to convergence as shown in figure 3. Comparing these results to the benchmarked PIV results reveals that Fluent's implementation of the $k-\varepsilon$ model is inadequate for correctly predicting the onset separation in this particular case.

3.2.2 30 FOOT SLAB CUT

A grid-independent solution was found for the 30 foot slab cut scenario using the $k-\varepsilon$ model with a standard wall function. Three grid sizes were solved to convergence as shown in figure 4. These results compare very well with the experimental data. One theory to explain this correlation is that the flow does not separate, thus it is very easy to compute. This case does not hold as much importance as the other three.

3.2.3 60 FOOT BOX CUT

A grid-independent solution was found for the 60 foot box cut scenario using the $k-\varepsilon$ model with a standard wall function. Three grid sizes were solved to convergence as shown in figure 5. Fluent did predict a separation of the flow near the same region in which PIV found separation. However, the separation was noticeably further down stream and the velocity seems to dissipate more rapidly than in PIV. This comparison can be considered a mild success because it did predict the separation, but apparent differences between Fluent and PIV prevent us from having confidence in Fluents ability to predict this scenario with accuracy.

3.2.4 60 FOOT SLAB CUT

A grid-independent solution was found for the 60 foot slab cut scenario using the $k-\varepsilon$ model with a standard wall function. Three grid sizes were solved to convergence as shown in figure 6. As no separation is predicted by Fluent, the comparison with experimental data shows no correlation. There, the implementation of the $k-\varepsilon$ model in the Fluent 6.0 package in inadequate for accurately predicting the onset separation found in this scenario.

3.3 The Spalart-Allmaras Model

3.3.1 30 FOOT BOX CUT

Although a grid-independent solution was not found while using the Spalart-Allmaras (S-A) turbulence model with the Fluent 6.0 package to compute the 30 foot box cut scenario, some promising results were discovered and are illustrated in figure 7. In sub-figure (a), the first order upwind scheme was used for a grid containing 1.2 million elements and the solution converged yielding a result that compares very well with PIV results. However, using the same grid and implementing the QUICK scheme, as seen in (b), which should yield a more accurate solution, the residuals begin to diverge. This leads us to believe that the stability of Fluent's implementation of the S-A model is unstable. Once more, as seen in (c), a coarse mesh using 800 thousand grid cells does converge yielding a solution that once again correlates very well with the experimental data. Therefore, for this scenario, we fear that Fluent's implementation of the S-A model is capable of predicting the correct solution, but may be very difficult to converge.

3.3.2 30 FOOT SLAB CUT

When modeling the 30 foot slab cut scenario using the S-A model and two different mesh densities, there were problems with converging the results. As seen in figure 8, only the coarse grid case actually yielded a reduction in the residual of more than $1.0E-3$ and the residual began to slope back up near $20,000$ iterations. Although the results from all three runs look similar to the experimental data, they cannot be trusted to the difficulty involved with converging Fluent's implementation of the S-A model. It should also be noted that this case is believed to be the easiest scenario to solve. Unlike the results from the 30 foot box cut scenario, not even the first order upwind scheme was able to converge this scenario.

3.3.3 60 FOOT BOX CUT

For the 60 foot box cut scenario five differently sized grids were attempted. As seen in figure 9(a), once again convergence became an issue with the computation. In figure 9(b) and (c), the residuals decreased below $1E-3$ but never settled into a flat line. Although the results from these two runs correlate well with the PIV data, the solutions stability is questionable. Next, in figure 10(a) the residual plot seemed to flatten but the curved still maintained an upward slope and some spikes. The large increase in the residual is explained by an increase in the under-relaxation factor. While the result for this case does predict a separation, it still does not compare well with the experimental data because the separation point is predicted much too far upstream in the flow. A similar result is shown in figure 10(b). Here the residual began to increase and a reduction of the under-relaxation factor falsely produced a drop in the residual and a stabilization in the plot. This produces evidence by reducing the under-relaxation factor, the user can produce a seemingly converged solution that is not truly converged. Therefore, it is concluded that Fluent's implementation of the S-A model is not stable enough to easily predict this scenario.

3.3.4 60 FOOT SLAB CUT

Many solutions are presented for the 30 foot slab cut scenario because this scenario is potentially the most difficult flow to predict. As shown in figure 11, three different grid densities were solved to convergence. Although, all three cases resulted in a separation of the flow, agreement between the cases could not be found. Instead, a trend was discovered such that the distance from the separation point to the face increases with the grid density. Thus, proving that the grid-independent solution has not been reached. Also, if this trend continues, correlation with the experimental data will never be found. Next, figure 12 shows a variety of cases in which the solution never converged. This again raises question to Fluent's implementation of the S-A model.

3.4 The $k-\omega$ SST Model

Only two scenarios have been modeled with the $k-\omega$ SST model. The 60 foot box cut and 60 foot slab cut have been modeled with one coarse mesh and one fairly fine mesh. The residuals and velocity vector plots can be seen in figures 13 and 14. As seen in the figures, even an extremely coarse mesh generated problems with stability. All of these solutions are invalid due to the lack of convergence and proper measures should be taken by the user to try to stabilize the residuals.

4 Conclusions

In conclusion, we have seen some problems with using the commercial software package Fluent to predict the onset separation that occurs during certain mining scenarios. It is shown that the solution is highly dependent on the grid and the selection of a turbulence model. We can conclude that if converged, the S-A model does predict the onset separation better than the $k-\varepsilon$. However, Fluent's limited ability to converge the S-A model, inconsistency in results yielded from the S-A model, and the lack of correlation between these results and experimental data suggests that the S-A model does not work well for the scenarios presented in this report.

5 Future Work

There is still much work to do before the completion of this project including:

further testing of the $k-\omega$ SST model, reduced height scenarios for comparison with PIV data, and testing with different software packages such as CFX 5.5.

- Complete Grid Sensitivity study for all scenarios using $k-\omega$ turbulence model.
- Test these cases with other commercial software such as *CFX* and *Star-CD*.
- Testing scenarios with a reduced height of 5.5 ft for comparison with PIV measurements
- Model the miner in the mine face and compare with PIV measurements.

6 Figures

6.1 Geometry for the Four Scenarios

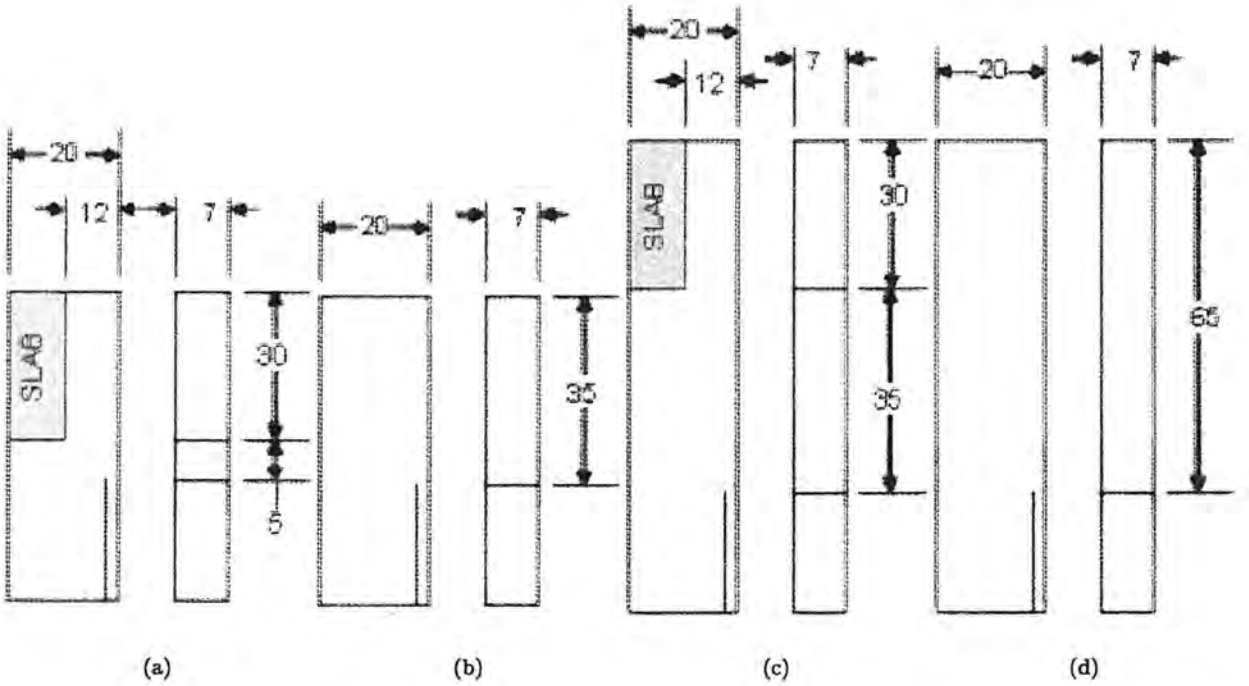

Figure 1: Geometry and dimensions for the four scenarios used to simulate the path of the miner. (a) 30 ft box cut, (b) 30 ft slab cut, (c) 60 ft box cut and (d) 60 ft slab cut.

6.2 Particle Image Velocimetry (PIV)

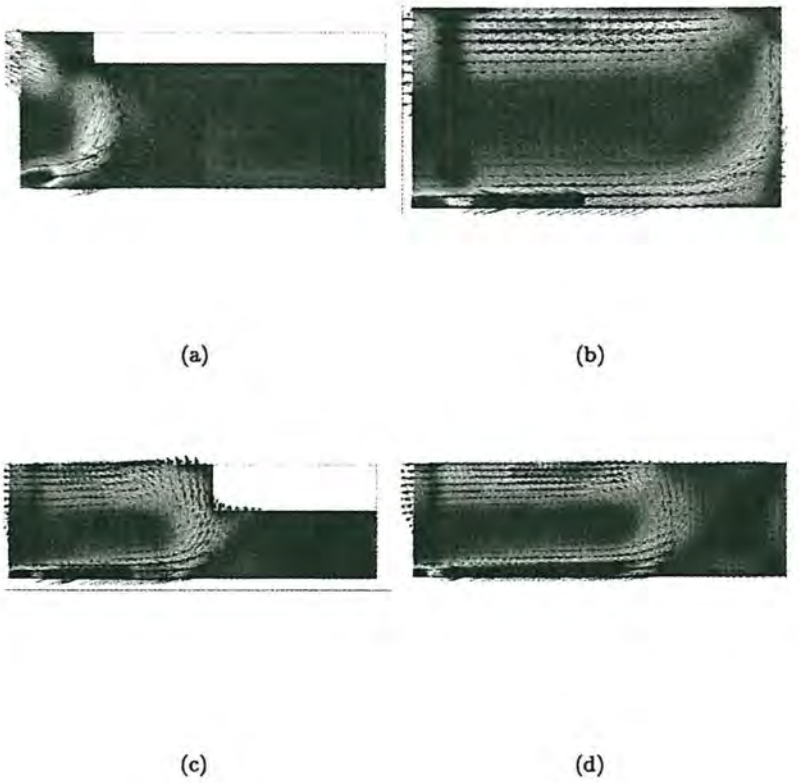

Figure 2: Velocity-vector plots for a) 30 foot box cut, b) 30 foot slab cut, c) 60 foot box cut and d) 60 foot slab cut, using the PIV experiments taken by Dr. Wala and Dr. Jacob.

6.3 The $k-\varepsilon$ Model with Standard Wall Function

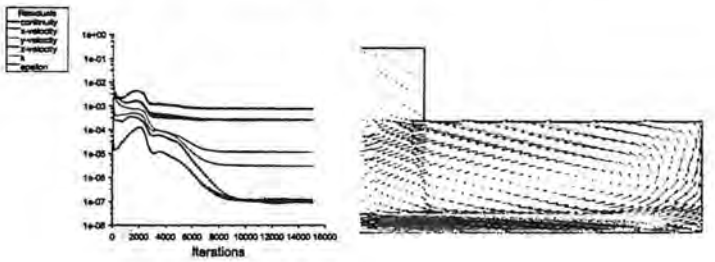

(a) 600 thousand grid cells, 1st order upwind

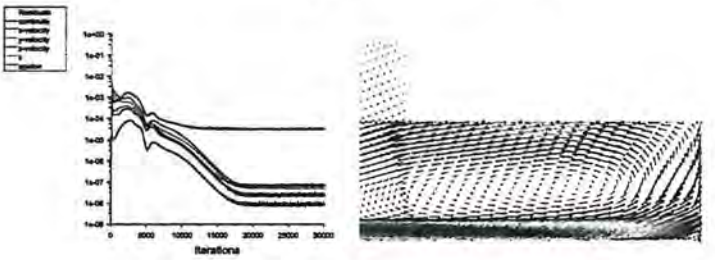

(b) 900 thousand, 1st order upwind

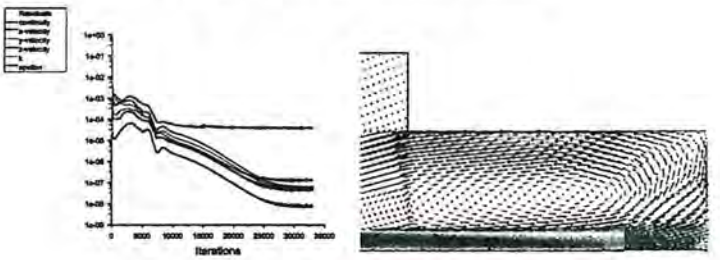

(c) 1.2 million grid cells, 1st order upwind

Figure 3: Residuals and velocity-vector plots for the 30 ft box cut scenario using the $k-\varepsilon$ turbulence model.

The $k-\varepsilon$ Model with Standard Wall Function continued

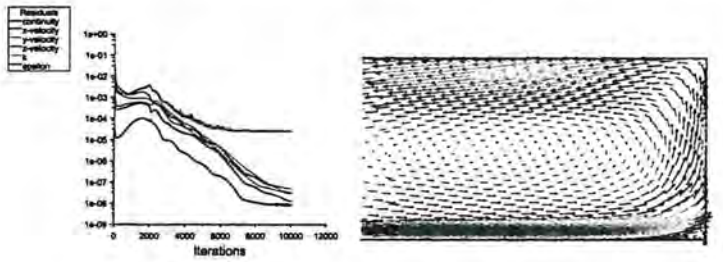

(a) 700 thousand grid cells, 1st order upwind scheme

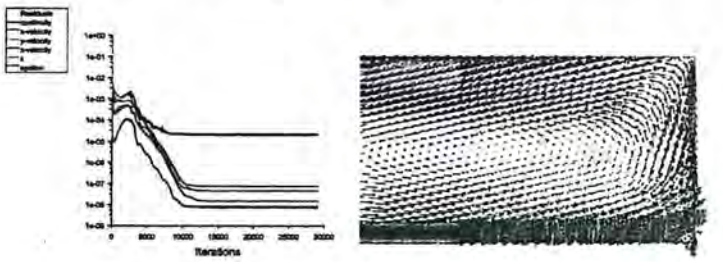

(b) 975 thousand grid cells, 1st order upwind scheme

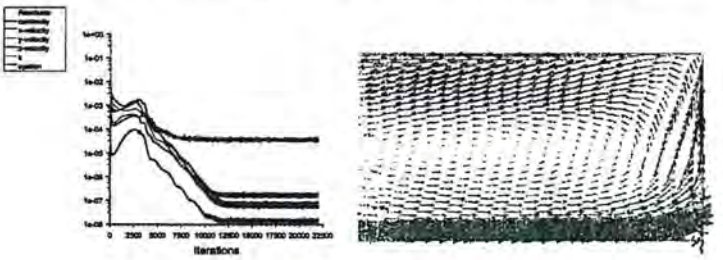

(c) 1.2 million grid cells, 1st order upwind scheme

Figure 4: Residuals and velocity-vector plots for the 30 ft slab cut scenario using the $k-\varepsilon$ turbulence model.

The $k-\varepsilon$ Model with Standard Wall Function continued

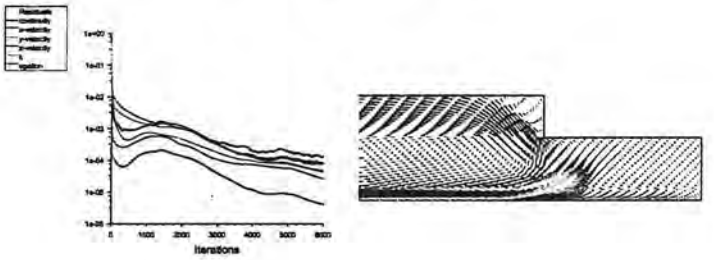

(a) 600 thousand grid cells, QUICK scheme

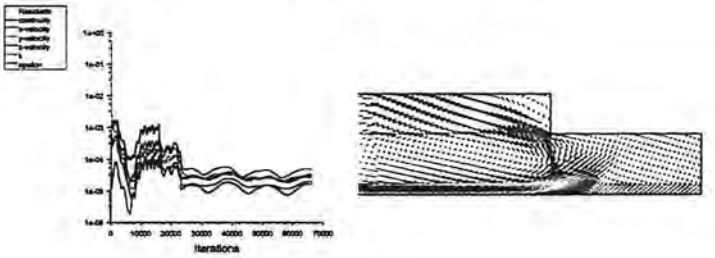

(b) 900 thousand grid cells, QUICK scheme

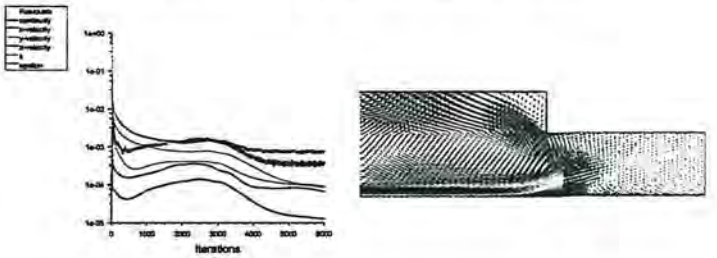

(c) 1.2 million grid cells, QUICK scheme

Figure 5: Residuals and velocity-vector plots for the 60 ft box cut scenario using the $k-\varepsilon$ turbulence model.

The $k-\varepsilon$ Model with Standard Wall Function continued

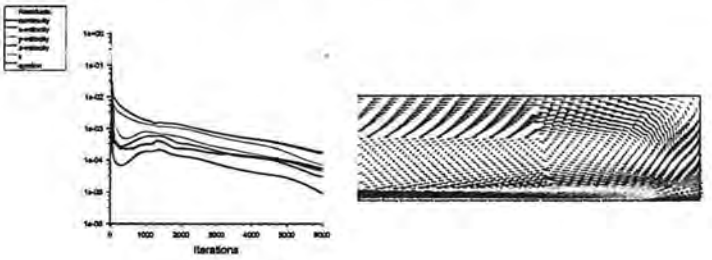

(a) 600 thousand grid cells, QUICK scheme

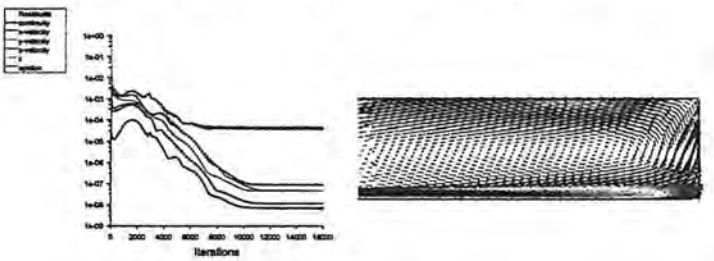

(b) 1.0 million grid cells, QUICK scheme

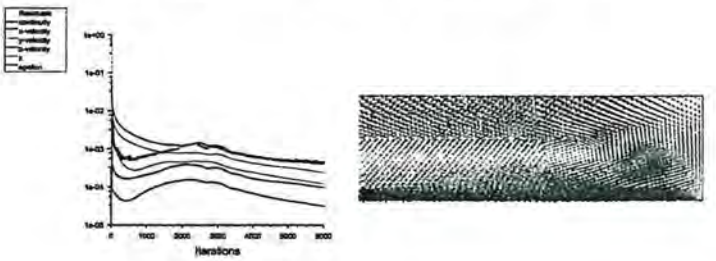

(c) 1.2 million grid cells, QUICK scheme

Figure 6: Residuals and velocity-vector plots for the 60 ft slab cut scenario using the $k-\varepsilon$ turbulence model.

6.4 The Spalart-Allmaras Model

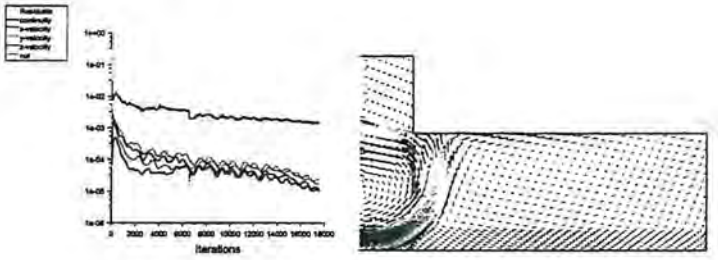

(a) 1.2 million grid points solved with first order upwind

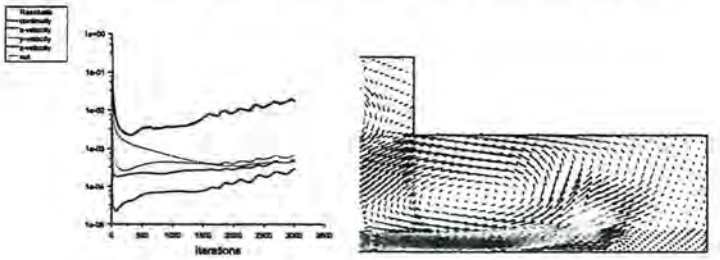

(b) 1.2 million grid points solved with the QUICK scheme.

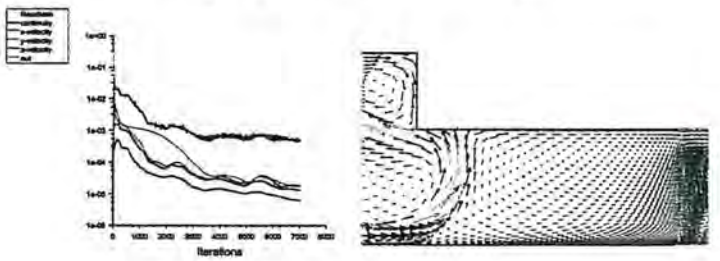

(c) 800K grid points solved using QUICK.

Figure 7: Residuals and velocity-vector plots for the 30 ft box cut scenario using the Spalart-Allmaras turbulence model.

The Spalart-Allmaras Model continued

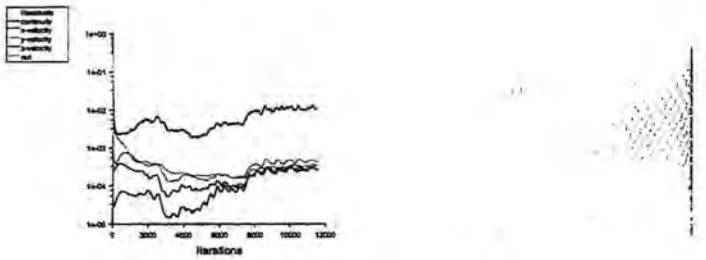

(a) 1.2 million grid points, first order upwind scheme

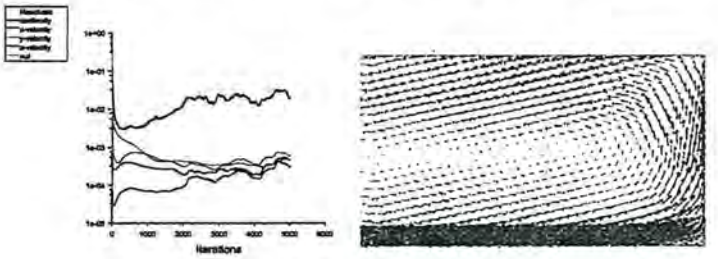

(b) 1.2 million grid points, QUICK scheme

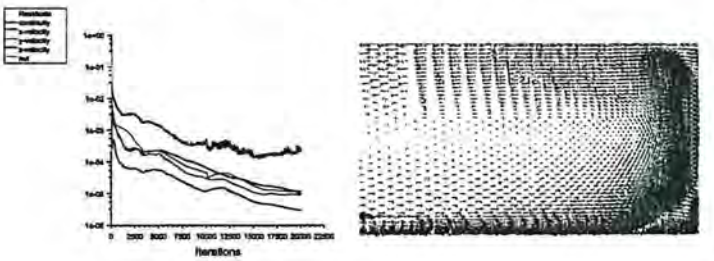

(c) 800K grid points, QUICK scheme

Figure 8: Residuals and velocity-vector plots for the 30 ft slab cut scenario using the Spalart-Allmaras turbulence model.

The Spalart-Allmaras Model continued

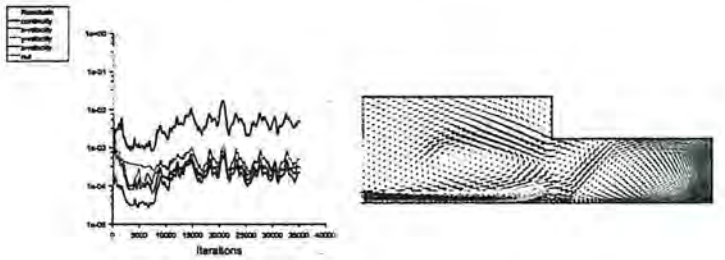

(a) 700 thousand grid cells, QUICK scheme

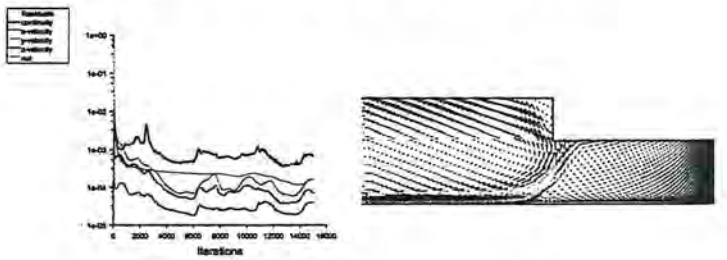

(b) 1.4 million grid cells, QUICK scheme

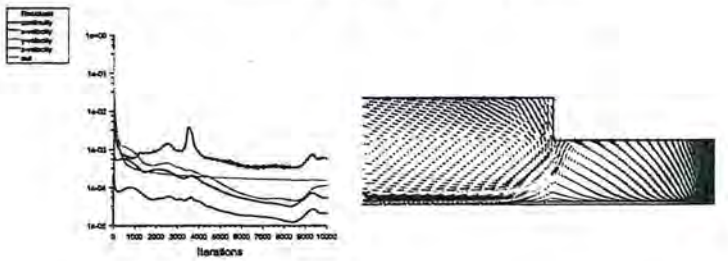

(c) 2.5 million grid cells, QUICK scheme

Figure 9: Residuals and velocity-vector plots for the 60 ft box cut scenario using the S-A turbulence model.

The Spalart-Allmaras Model continued

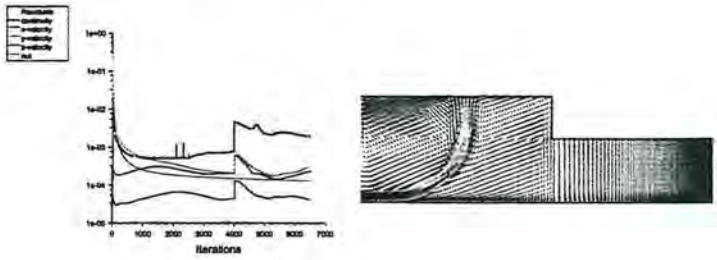

(a) 1.5 million grid cells, QUICK scheme

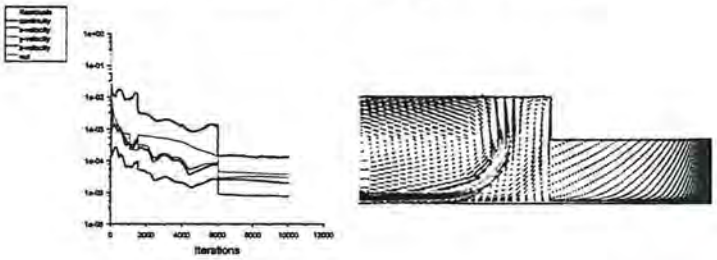

(b) 2.2 million grid cells, QUICK scheme

Figure 10: Residuals and velocity-vector plots for the 60 ft box cut scenario using the S-A turbulence model.

The Spalart-Allmaras Model continued

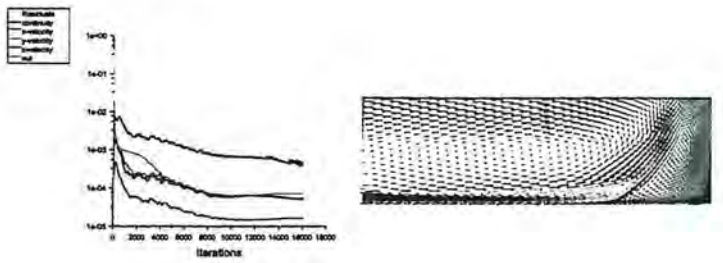

(a) 950 thousand grid cells, QUICK scheme

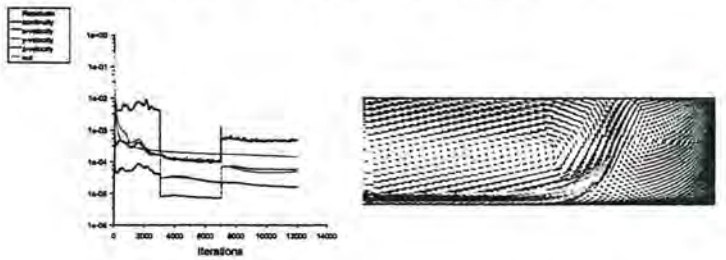

(b) 1.8 million grid cells, QUICK scheme

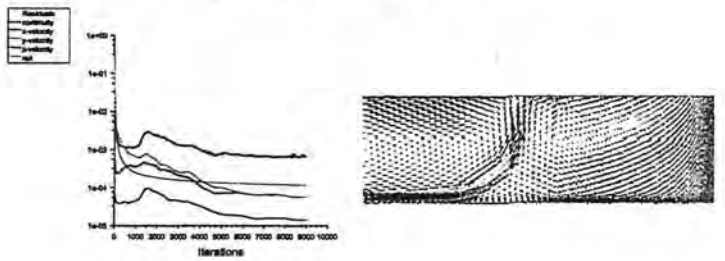

(c) 3.0 million grid cells, QUICK scheme

Figure 11: Residuals and velocity-vector plots for the 60 ft slab cut scenario using the S-A turbulence model.

The Spalart-Allmaras Model continued

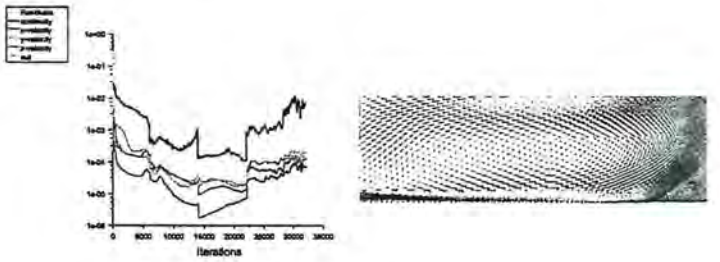

(a) 700 thousand grid cells, QUICK scheme

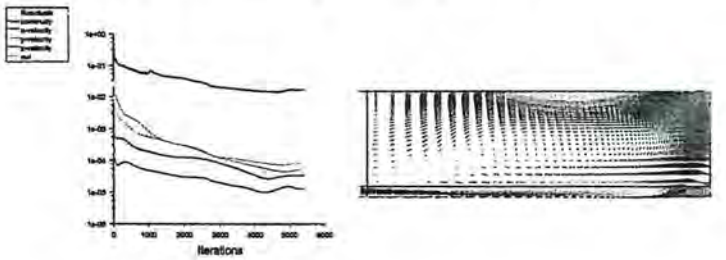

(b) 2.0 million grid cells, QUICK scheme

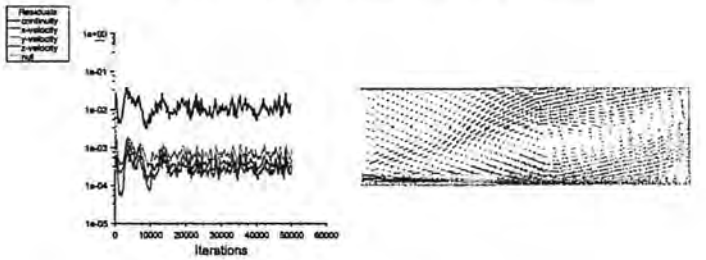

(c) 300 thousand grid cells, QUICK scheme

Figure 12: Residuals and velocity-vector plots for the 60 ft slab cut scenario using the S-A turbulence model.

6.5 The $k-\omega$ SST Model

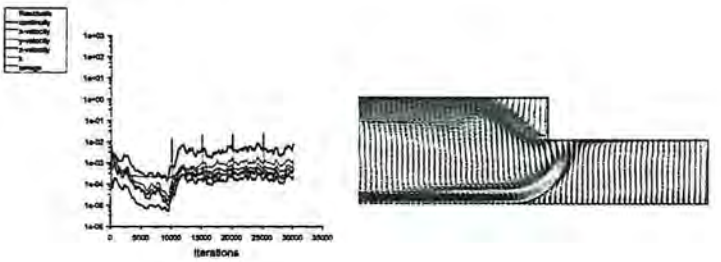

(a) 270 thousand grid cells, QUICK scheme

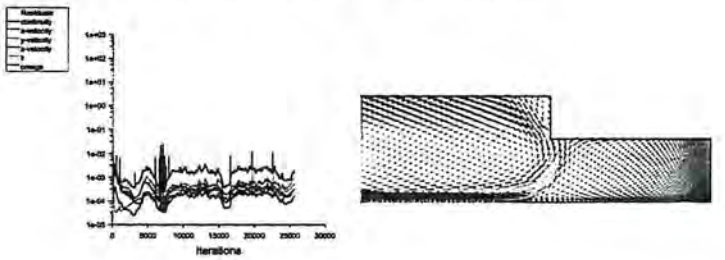

(b) 700 thousand grid cells, QUICK scheme

Figure 13: Residuals and velocity-vector plots for the 60 ft box cut scenario using the $k-\omega$ SST turbulence model.

The $k-\omega$ SST Model continued

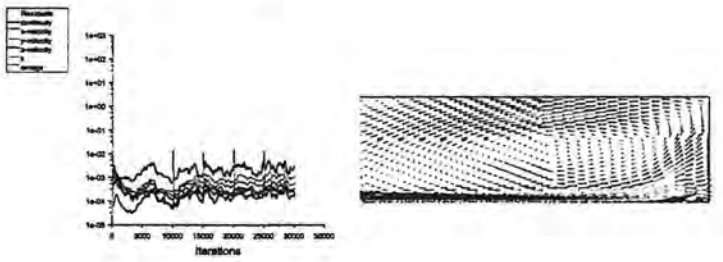

(a) 300 thousand grid cells, QUICK scheme

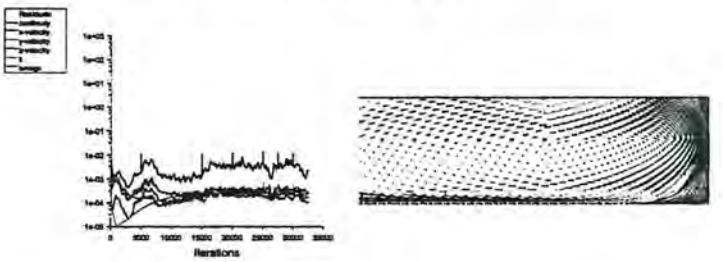

(b) 950 thousand grid cells, QUICK scheme

Figure 14: Residuals and velocity-vector plots for the 60 ft slab cut scenario using the $k-\omega$ SST turbulence model.

References

[1] Wala, Andrezj, Jacob, J.D., Huang, G.P., and Brown J.T. Numerical and Experimental Study of a Mine Face Ventilation System for CFD Validation. A Pre-Print of the 2002 SME Annual Meeting in Phoenix, AZ.

[2] Fluent User's Guide

[3] Wilcox, David C. BASIC FLUID MECHANICS. DCW Industries, Inc. First Edition. 1997. Pages 1-13.